SCIENTIFIC REPORTS

OPEN

SUBJECT AREAS:
MAGNETIC PROPERTIES AND MATERIALS
ELECTRONIC PROPERTIES AND MATERIALS
SUPERCONDUCTING PROPERTIES AND MATERIALS

Received
20 August 2013

Accepted
30 September 2013

Published
15 October 2013

Correspondence and requests for materials should be addressed to Z.Q.M. (zmao@tulane.edu)

Competition Between Antiferromagnetism and Ferromagnetism in Sr_2RuO_4 Probed by Mn and Co Doping

J. E. Ortmann[1], J. Y. Liu[1], J. Hu[1], M. Zhu[2], J. Peng[1], M. Matsuda[3], X. Ke[2] & Z. Q. Mao[1]

[1]Department of Physics and Engineering Physics, Tulane University, New Orleans, Louisiana 70118, USA, [2]Department of Physics and Astronomy, Michigan State University, East Lansing, Michigan 48824, USA, [3]Quantum Condensed Matter Division, Oak Ridge National Laboratory, Oak Ridge, Tennessee 37831, USA.

Spin-triplet superconductivity in Sr_2RuO_4 has attracted enormous interest. Like other unconventional superconductors, superconductivity in Sr_2RuO_4 is in close proximity to magnetic instability. Undoped Sr_2RuO_4 exhibits incommensurate antiferromagnetic (AFM) fluctuations, which can evolve into static, short-range AFM order via Ti doping. Moreover, weak ferromagnetic (FM) coupling in Sr_2RuO_4 has also been suggested by NMR/neutron scattering experiments and studies on $Ca_{2-x}Sr_xRuO_4$ and $Sr_{2-y}La_yRuO_4$, implying orbital dependent magnetism. We report bulk static, short-range FM order in Sr_2RuO_4 triggered by $<2\%$ Co doping, showing superconductivity in Sr_2RuO_4 is much closer to FM instability than previously reported in $Ca_{2-x}Sr_xRuO_4$. We also find Mn doping can effectively establish incommensurate AFM order, with $T_N \sim 50$ K for 3% Mn doping. These new results place Sr_2RuO_4 in a unique situation where superconductivity lies directly on the borderline of two distinct magnetic states, highlighting the important role of competing magnetic fluctuations in determining superconducting properties of Sr_2RuO_4.

Shortly after the discovery of superconductivity at $T_c \sim 1.5$ K in Sr_2RuO_4[1], it was proposed that the superconductivity of this material may involve an unconventional pairing symmetry[2–5]. Rice and Sigrist[6] proposed a phenomenological model of spin triplet p-wave superconductivity in Sr_2RuO_4 based on the similarities of the Fermi liquid states of Sr_2RuO_4 and liquid ^{3}He as well as the ferromagnetism of relative compound $SrRuO_3$. The notion of spin-triplet superconductivity in Sr_2RuO_4 has now been demonstrated by several key experiments[7–9] and exotic properties arising from spin-triplet pairing have been observed in a growing number of experiments, such as time-reversal symmetry breaking[7,10], chiral order parameter domain[11] and half-quantum fluxoid states[12]. However, there is still no clear agreement on the exact nature of the mechanism responsible for this unconventional pairing symmetry and interest in this question has generated considerable research over the last 15 years[13,14].

In many unconventional superconductors, such as high-T_c cuprates[15], iron pnictides[16], and heavy Fermion systems[17], the superconducting state lies adjacent to static magnetic order. Such close proximity of the superconducting state to static magnetic order has naturally led to the suggestion that spin fluctuations may play a key role in the pairing mechanism of these unconventional superconductors. Given that Sr_2RuO_4 shows spin-triplet superconductivity, it is natural to ask whether or not its superconducting state also lies adjacent to static magnetic order. A great deal of work has been done to address this question. Early inelastic neutron scattering studies of Sr_2RuO_4 found evidence for incommensurate spin fluctuations at the wavevector $\boldsymbol{Q}_{ic} \approx (\pm 2\pi/3a, \pm 2\pi/3a, 0)$[18], consistent with the theoretical prediction of spin-density-wave (SDW) magnetic fluctuations driven by Fermi surface nesting between the α and β sheets derived from Ru $4d_{xz/yz}$ orbitals[19]. Such incommensurate magnetic fluctuations can be stabilized by Ti doping[20] and short-range, static incommensurate order was probed in neutron scattering measurements of the 9% Ti-doped sample[21]. Although these results have established that Sr_2RuO_4 is adjacent to incommensurate magnetic order, AFM fluctuations are expected to favor d-wave pairing over p-wave pairing[19]. According to the phenomenological theory by Rice and Sigrist[6] and theoretical studies by several other groups[22–25], ferromagnetic (FM) fluctuations are in favor of p-wave pairing. The first-principles calculations by Mazin and Singh suggest that Sr_2RuO_4 may possess FM fluctuations due to the fact that the Fermi-level of Ru $4d_{xy}$

bands is close to a van Hove singularity (vHS)[22]. The evidence for FM coupling in undoped Sr_2RuO_4 was first observed in ^{17}O and ^{101}Ru NMR measurements by Imai *et al.*[26], which showed that the spin correlations from Ru $4d_{xy}$ orbitals are predominantly FM in nature. Nevertheless, later inelastic neutron scattering measurements on Sr_2RuO_4, while showing some evidence of magnetic excitation at zone center, suggest that FM fluctuations in Sr_2RuO_4 are very weak[27].

Given that weak FM fluctuations coexist with incommensurate fluctuations in Sr_2RuO_4, one may expect a scenario where chemical doping can band selectively enhance FM fluctuations or even trigger static FM order as Ti doping selectively stabilizes the incommensurate order. Such a possibility has been examined by Kikugawa *et al.*[28,29]. They found that La^{3+} substitution of Sr^{2+} in Sr_2RuO_4 enhances FM fluctuations; this result has been interpreted in terms of the electron doping from La^{3+} bringing the Fermi level of Ru $4d_{xy}$ bands close to the vHS. Also, a new phase diagram of $Ca_{2-x}Sr_xRuO_4$ recently established by μSR measurements[30] reveals that a FM cluster glass discovered previously[31] near $x = 0.5$ indeed extends to $x = 1.5$. Coexistence of phases with and without spin freezing is observed even in the $x = 1.8$ sample. These results imply that Sr_2RuO_4 is not far from an FM instability. Given the important role FM fluctuations are expected to play in the pairing mechanism and the observation that AFM order can be induced by a small amount of doping, it is natural to ask if FM order can also be induced in Sr_2RuO_4 with relatively little doping. In this Report, we show that Sr_2RuO_4 is indeed right on the borderline of short-range static FM order. As little as 0.8–1.5% Co doping in Sr_2RuO_4 can trigger static, short-range FM order. Furthermore, we find that Mn doping can enhance the incommensurate order much more significantly than Ti doping; 3% Mn doping can establish static incommensurate order with $T_N \sim$ 50 K, as opposed to $T_N \sim 25$ K in the 9% Ti-doped sample[21]. These new results underline the strong competition between ferromagnetism and antiferromagnetism in Sr_2RuO_4 and point toward the important role of magnetic fluctuations in mediating the superconducting pairing.

Results

We present magnetic susceptibility data of Mn-doped samples in Fig. 1a where the data of undoped Sr_2RuO_4 is also given for comparison. All Mn-doped samples show irreversibility between zero-field cooled (ZFC) and field-cooled (FC) histories in susceptibility at low temperatures for field parallel *c*, but not for field parallel *ab*, indicating that Mn doping induces striking Ising anisotropy in Sr_2RuO_4. This observation is reminiscent of Ti-doped Sr_2RuO_4, which exhibits similar history dependence in magnetic susceptibility[20]. The susceptibility irreversibility in Ti-doped Sr_2RuO_4 has been shown to originate from a spin glass state at low temperatures[20]. To verify if the history dependence of susceptibility observed in Mn-doped Sr_2RuO_4 is also associated with a spin glass state, we examined the relaxation of magnetization of Mn-doped samples. In general, significant magnetic relaxation is a signature of a spin glass state. Like Ti-doped Sr_2RuO_4, the Mn-doped samples indeed exhibit remarkable magnetic relaxation below the temperature T_{ir} where the irreversible behavior of susceptibility begins. Fig. 1b shows magnetic relaxation data collected on the sample with 10% Mn at various temperatures; T_{ir} of this sample is ~40 K.

Furthermore, we also measured the initial remnant magnetization M_0 as a function of temperature for all Mn-doped samples. M_0 data was collected by first zero-field-cooling the sample to a given temperature from 300 K, then applying a magnetic field of 5 T for 300 seconds and decreasing the field to zero. As seen in Fig. 1c, we observed a pronounced peak in $M_0(T)$ for the 10% Mn-doped sample at a temperature slightly below T_{ir}, a feature similar to what was observed in Ti-doped Sr_2RuO_4[20]. As mentioned in the introduction, the spin-glass state in Ti-doped Sr_2RuO_4 is characterized by short-range incommensurate AFM order. Given that Mn-doped samples

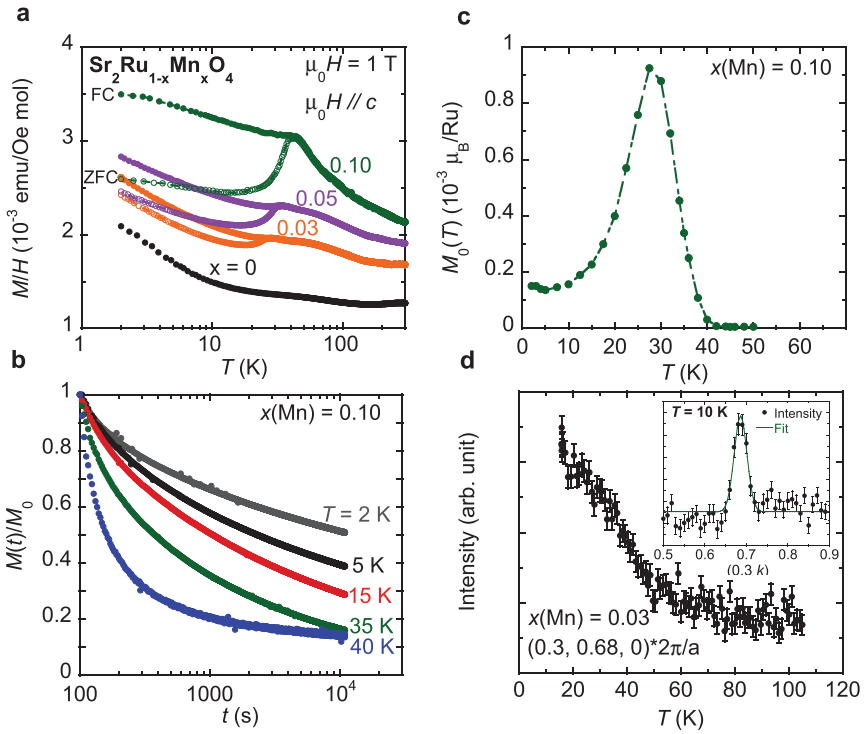

Figure 1 | Magnetic properties of $Sr_2Ru_{1-x}Mn_xO_4$. (a) Magnetic susceptibility vs. temperature measured with ZFC and FC histories; (b) time dependence of remnant magnetization, measured after first zero-field-cooling the sample to a given temperature from 300 K, then applying a magnetic field of 5 T for 300 seconds and decreasing the field to zero; (c) initial remnant magnetization M_0, *i.e.* $M(t = 0)$, vs. temperature for 10% Mn-doped sample; (d) temperature dependence of the neutron scattering intensity of the magnetic Bragg peak at (0.3,0.68,0)*(2π/a) for 3% Mn-doped sample, inset: the magnetic Bragg peak at (0.3,0.68,0)*(2π/a).

and Ti-doped samples show strikingly similar magnetic behavior in the measurements discussed so far, it is reasonable to expect a similar spin glass state with short-range incommensurate order in Mn-doped samples. Indeed, this has been confirmed by our elastic neutron scattering measurements shown in Fig. 1d, where a magnetic Bragg peak at (0.3, 0.68, 0)*2π/a (inset) as well as the peak intensity temperature dependence are presented. These data clearly show 3% Mn-doped Sr_2RuO_4 forms incommensurate AFM order below $T_N \sim$ 50 K with an almost identical ordering wavevector to that found in Ti-doped Sr_2RuO_4[21]. It is worth noting that Mn doping is much more effective than Ti doping at inducing incommensurate AFM order. The Néel temperature of 3% Mn-doped sample is approximately twice that of 9% Ti-doped sample ($T_N \sim$ 25 K), indicating the AFM coupling is stronger in the Mn-doped system than in the Ti-doped system.

In Fig. 2a, we present magnetic susceptibility for Co-doped Sr_2RuO_4. Like Mn- and Ti-doped samples, Co-doped samples also show Ising anisotropy in susceptibility, with irreversibility between ZFC and FC histories apparent for field parallel *c*. T_{ir} is ~4 K and 10 K, respectively, for 0.8% and 1.5% Co doping. Moreover, Co-doped Sr_2RuO_4 also shows relaxation of remnant magnetization below T_{ir}, as shown in Fig. 2b. These features indicate that Co doping also leads to a low-temperature glassy state in Sr_2RuO_4. However, the nature of the glassy state in the Co-doped sample is distinct from that in the Mn-doped sample, as implied by comparing the initial remnant magnetization $M_0(T)$ for these two materials shown in Fig. 2c and 1c, respectively. Rather than a pronounced peak in $M_0(T)$ as seen in the Mn- and Ti-doped samples, the Co-doped sample shows a monotonic, steep increase in M_0 with decreasing temperature for $T < T_{ir}$ (Fig. 2c). The difference in magnitude of M_0 at the lowest temperatures is also remarkable: $M_0(T = 2\ K)$ for the 1.5% Co-doped sample is ~35 times greater than $M_0(T = 2\ K)$ for the 10% Mn-doped sample. These observations suggest that Co-doped Sr_2RuO_4 may form an FM cluster glass rather than a spin glass with incommensurate AFM order, as seen in the Mn-doped samples. This is indeed verified by the magnetic hysteresis as well as the exponential magnetic relaxation, as discussed below. As shown in Fig. 2d, with as little as 1.5% Co doping, the isothermal magnetization data shows significant hysteresis with a coercive force >0.50 T and remnant magnetization of ~6.5 $m\mu_B$/Ru. Such hysteric behavior of magnetization develops only when the temperature is lowered below T_{ir} (~10 K). The 0.8% Co-doped sample also shows hysteresis, although it is not as dramatic as that observed in the 1.5% Co-doped sample. In contrast, none of the Mn-doped samples studied show hysteresis in isothermal magnetization data and instead show linear field dependence, as seen in the 10% Mn-doped sample in Fig. 2d. The presence of magnetic hysteresis in the Co-doped samples clearly indicates the formation of static FM order. Such FM order should represent a short-range order, since the Arrott plot of magnetization for 1.5% Co-doped sample does not show any spontaneous magnetization for $T < T_{ir}$, which is the hallmark of a long-range FM order (see Supplementary Information S1). The notion of short-range order is also consistent with the observed susceptibility data, which does not show the sharp increase usually associated with the onset of long-range FM order, but rather shows a crossover to irreversibility below T_{ir}.

The FM cluster glass state in the Co-doped sample is also manifested in the exponential magnetic relaxation. As shown in the inset of Fig. 2b, the time dependence of magnetization for the 1.5% Co-doped sample can be best described by $M(t) \propto \exp[-(t/\tau)^{0.06}]$, where $\tau \sim 7.8 \times 10^5$ s, which resembles the exponential magnetic relaxation of the FM cluster phase observed in $Ca_{1.5}Sr_{0.5}RuO_4$, where $M(t) \propto \exp[-(t/\tau)^{0.26}]$ ($\tau \sim$ 2800 s)[31]. The large difference in τ and the exponent between these two systems should be attributed to the

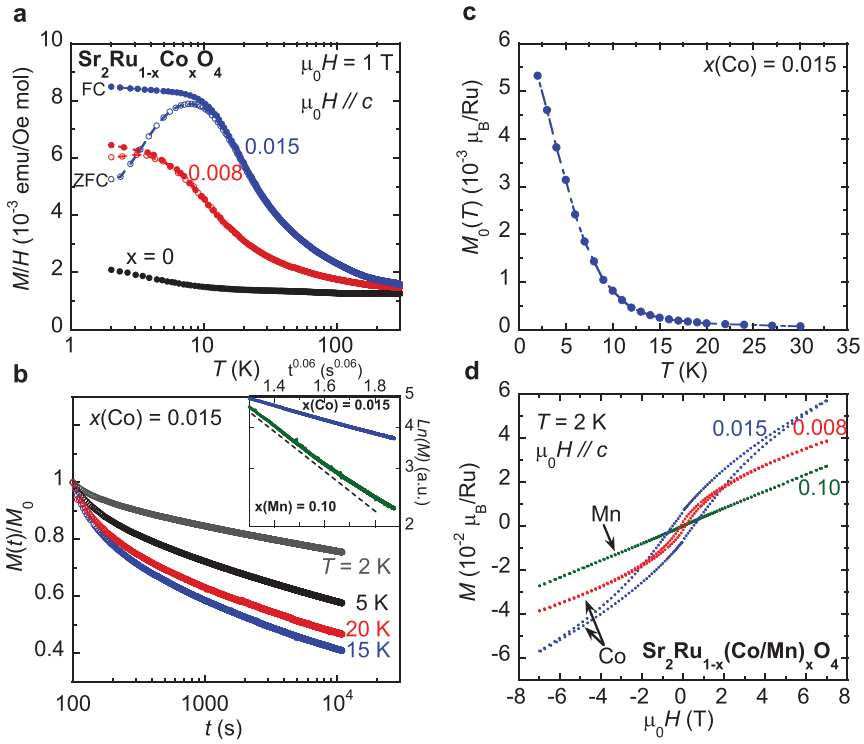

Figure 2 | Magnetic properties of $Sr_2Ru_{1-x}Co_xO_4$. (a) Magnetic susceptibility vs. temperature measured with ZFC and FC histories. (b) Time dependence of magnetization, measured after first zero-field-cooling the sample to a given temperature from 300 K, then applying a magnetic field of 5 T for 300 seconds and decreasing the field to zero. Inset: relaxation curve of *M* (on logarithmic scale) at 2 K for 1.5% Co- and 10% Mn-doped samples; the dashed linear line in the inset is used as a reference to show the $M(t)$ for the 10% Mn-doped sample slightly deviates from linearity. (c) Initial remnant magnetization M_0, *i.e.* $M(t = 0)$, vs. temperature for 1.5% Co-doped sample. (d) Isothermal magnetization data for 0.8% Co-, 1.5% Co- and 10% Mn-doped samples.

difference in FM coupling strength and the different temperature at which measurements were performed. In contrast, $M(t)$ for the Mn-doped sample neither follows the exponential time dependence that the Co-doped sample follows (as shown in the inset of Fig. 2b), nor shows ln(t) dependence as the Ti-doped sample does (see Fig. 1b)[20]; this is in line with our expectation that the glassy states of Co- and Mn-doped samples are distinct.

It is important to stress that the weak ferromagnetism seen in magnetization measurements of Co-doped samples is not due to intergrowth of FM relative compound $SrRuO_3$, as made clear by a few key observations. First, the Curie temperature T_c of $SrRuO_3$ is 160 K for the bulk material[32] and in the 110–160 K range for the phase at nanometer length scale[33]. Our susceptibility measurements show no features between 110 K and 160 K. Because the SQUID magnetometer is extremely sensitive to FM phases, the absence of any FM response in the 110–160 K range indicates that $SrRuO_3$ intergrowth is negligible in our samples. Secondly, as noted above, the Arrott plot for 1.5% Co-doped Sr_2RuO_4 does not show spontaneous magnetization, which is inconsistent with the long-range FM order seen in $SrRuO_3$. Finally, we have purposely measured undoped crystals with significant $SrRuO_3$ intergrowth and found these mixed phase samples do not show magnetic relaxation behavior (see Supplementary Information S2), in contrast with the observation of magnetic relaxation in Co-doped samples. From all these observations, we conclude the FM response in our Co-doped crystals is purely an effect of doping and is not due to FM $SrRuO_3$ intergrowth.

Co and Mn doping in Sr_2RuO_4 not only lead to two different spin glass states as discussed above, but also cause distinct electronic states, as evidenced by resistivity data presented in Fig. 3. For Mn-doped samples, we observe a low-temperature upturn for both in-plane (ρ_{ab}) and out-of-plane (ρ_c) resistivity at the same temperature. Although the resistivity values of the Mn-doped samples are relatively small (e.g. $\rho_{ab} \sim 7.5 \times 10^{-5}\ \Omega$ cm at 2 K for 3% Mn-doping), this upturn indicates that Mn doping leads to a weakly localized state,

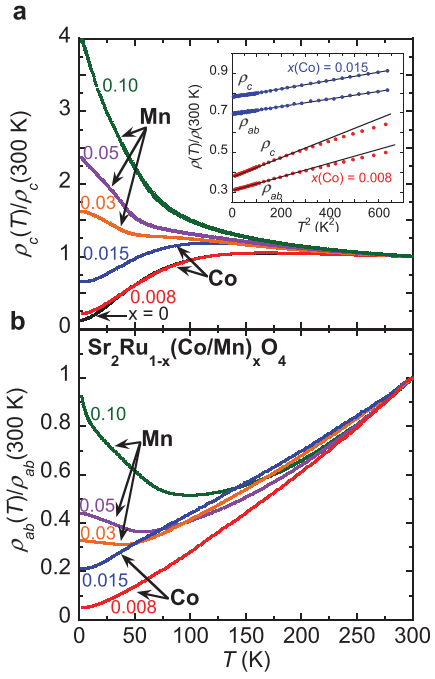

Figure 3 | Electronic transport properties of $Sr_2Ru_{1-x}(Co/Mn)_xO_4$. Out-of-plane (a) and in-plane (b) resistivity, normalized to room temperature resistivity. The low-temperature weakly localized state of the Mn-doped samples is apparent for both current orientations. The inset in (a) shows in-plane and out-of-plane resistivity vs. T^2 for 0.8% and 1.5% Co-doped Sr_2RuO_4.

as seen in Ti-doped samples[20]. To examine if such a low-temperature upturn of resistivity is associated with the Kondo effect, we have plotted the resistivity on the logarithmic scale of temperature (see Supplementary Information S3). We do not observe the expected log(T) dependence, which excludes the possibility that Mn doping results in a Kondo effect. The onset of the weakly localized state is much higher than the irreversibility temperature T_{ir} determined from magnetization measurements, but coincides with the onset temperature of incommensurate order probed in neutron scattering, both occurring at ~50 K in the 3% Mn-doped sample. We note that the weakly localized state in Ti-doped Sr_2RuO_4 also begins at approximately the same temperature as incommensurate order begins to form in the system[20,21]. This suggests that local moments may play a role in the formation of static AFM order in both the Ti-doped system and the Mn-doped system. This will be discussed further below.

In contrast to Mn and Ti impurities, we see from the resistivity data in Fig. 3 that Co impurities are apparently not strong scattering centers in Sr_2RuO_4: ρ_{ab} remains metallic all the way down to 2 K and ρ_c is also metallic below ~120 K in both Co-doped samples. Both ρ_{ab} and ρ_c exhibit quadratic temperature dependences at low temperatures as shown in the inset of Fig. 3a, indicating that a Fermi liquid ground state, which is seen in undoped Sr_2RuO_4, survives in Co-doped samples. This is in sharp contrast to the weakly localized state seen at low temperatures for both Ti- and Mn-doped Sr_2RuO_4. Given that the presence of static incommensurate order is always accompanied with a weakly localized electronic state in Mn- and Ti-doped samples, the observation of Fermi liquid behavior of resistivity in Co-doped samples implies that Co doping does not induce static incommensurate order except for the short-range FM order. From our preliminary neutron scattering measurements on the 3% Co-doped sample, we indeed did not observe any signature of static incommensurate order.

In Figure 4a we present a magnetic phase diagram for Mn- and Co-doped Sr_2RuO_4, which is established by the magnetization, resistivity and neutron scattering measurements described above. Symbols "◆" and "●" represent characteristic temperatures defined from susceptibility irreversibility (T_{ir}) and resistivity upturn (T_{WL}), respectively. The incommensurate ordering temperature T_N probed by neutron scattering in the 3% Mn-doped sample is also added to the diagram. It can be clearly seen that T_N is approximately equal to T_{WL}, but much higher than T_{ir} for this sample. Such a large discrepancy between T_N and T_{ir} is also observed in the spin glass state of Ti-doped Sr_2RuO_4 and is explained in terms of a crossover transition from damped inelastic magnetic fluctuations to elastic magnetic order[21]. This interpretation should also be applicable to Mn-doped samples. That is, T_N probed in neutron scattering should represent the onset of damped incommensurate fluctuations, while T_{ir} corresponds to the onset of static order. Given that $T_{WL} \approx T_N$ for the 3% Mn-doped sample and Ti doped samples[20,21], we can reasonably use T_{WL} to track the incommensurate ordering in other Mn-doped samples. Following this definition, T_N for the 10% Mn-doped sample is estimated to be ~75 K. For Co doped samples, T_{ir} should correspond to the onset of FM cluster glass as indicated above.

Discussion

The phase diagram in Fig. 4a shows the surprising result that superconductivity in Sr_2RuO_4 is *directly* adjacent to *both* static incommensurate AFM order and static FM order. Notably, this phase diagram shows that superconductivity in Sr_2RuO_4 is much closer to the FM instability, as compared to the $Ca_{2-x}Sr_xRuO_4$ phase diagram where bulk FM cluster glass phase does not appear until $x = 1.5$[30]. The fact that bulk static, short-range FM and AFM orders can be induced by <2% Co doping and 3% Mn doping, respectively, in Sr_2RuO_4 unambiguously demonstrates that Sr_2RuO_4 is in close proximity to distinct magnetically ordered states. This is in stark contrast with

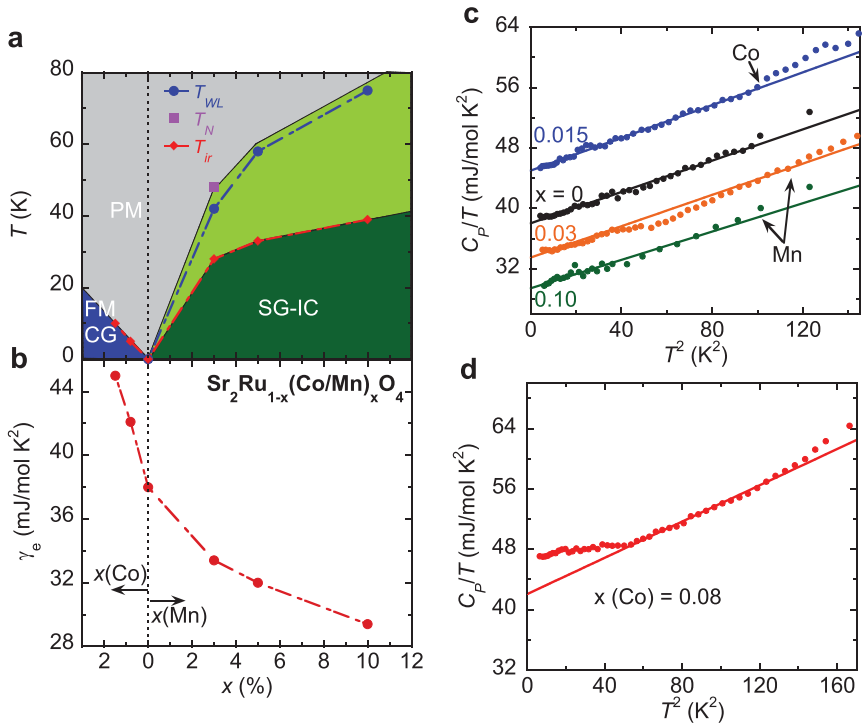

Figure 4 | Magnetic phase diagram and specific heat data of $Sr_2Ru_{1-x}(Co/Mn)_xO_4$. (a) Magnetic phase diagram; PM: paramagnetic, FM CG: ferromagnetic cluster glass, SG-IC: spin glass state with short-range incommensurate antiferromagnetic order. (b) Doping dependence of Sommerfeld coefficient γ_e. (c) Specific heat C divided by temperature vs. T^2 for undoped, 1.5% Co-, 3% Mn- and 10% Mn-doped samples. The solid lines represent linear fits. (d) Specific heat C divided by temperature vs. T^2 for the 0.8% Co-doped sample; the best linear fit (*i.e.* the solid line) is obtained in the 7–12 K temperature range.

other unconventional superconductors, which are normally adjacent to only *one* ordered state, as mentioned above. The close proximity to two competing magnetic states places Sr_2RuO_4 in a very unique situation where superconductivity may depend on competing AFM and FM fluctuations as discussed by Singh and Mazin previously[19]. Since such competing magnetic fluctuations most likely come from a multiple band effect[19], they may account for unusual superconducting properties in Sr_2RuO_4, such as orbital-dependent superconductivity[3,34,35]. The fact that such a small amount of doping can trigger bulk, static magnetic order in our materials also highlights the strong electron correlation effect present in Sr_2RuO_4.

Why do Co and Mn doping induce two distinct magnetic states in Sr_2RuO_4? Why can static magnetic order be established at such a low doping concentration in both scenarios? The answers to these questions are apparently instrumental to understanding of spin-triplet superconductivity in Sr_2RuO_4. Before we address these questions, let's first briefly summarize the current understanding of the spin-glass states induced by Ti doping[20] and Ca substitution for Sr[30,31], as well as enhanced FM fluctuations caused by La substitution for Sr[28,29]. As indicated above, the spin glass state in $Ca_{2-x}Sr_xRuO_4$ is characterized by short-range FM order. It stems from structural distortion caused by Ca substitution for Sr. Since Ca^{2+} has a smaller ionic radius than Sr^{2+}, Ca^{2+} substitution for Sr^{2+} leads to RuO_6 octahedral rotation for $0.5 \leq x < 1.5$, and simultaneous rotation and tilting for $0 \leq x < 0.5$[36]. First principle calculations revealed that the RuO_6 octahedral rotation leads to band narrowing and an increase in the density of states (DOS) at the Fermi level, $N(E_F)$[24], which enhances FM correlation according to Stoner criterion. For La-substituted Sr_2RuO_4, enhanced FM fluctuations can be attributed to the increase of $N(E_F)$ arising from electron doping as noted above[28,29]. As for the spin glass state with short-range AFM order stabilized by Ti doping, there are two possible mechanisms: a) since incommensurate magnetic fluctuations in Sr_2RuO_4 are thought to be driven by FS nesting[19], the static incommensurate order caused by Ti doping may be attributed to the improved FS nesting, or b) the incommensurate order may be associated with local moment magnetism, as pointed out in Ref. 37.

Next, let's examine if the Co and Mn doping effects can be understood in term of the existing knowledge stated above. First, given the FM cluster glass forms at <2% Co doping, the structural change caused by doping is nearly negligible, as seen in our x-ray diffraction analyses. Hence the enhancement of FM correlation in Co-doped samples should not be attributed to the structural distortion as in $Ca_{2-x}Sr_xRuO_4$. However, Co doping should lead to electron doping, since Co and Ru have different chemical valence and the 3d orbital of Co^{2+} ($3d^7$) or Co^{3+} ($3d^6$) has more electrons than the 4d orbital of Ru^{4+} ($4d^4$). If the enhanced FM correlation in Co-doped Sr_2RuO_4 turns out to be from the band filling as in La-substituted Sr_2RuO_4, we would naturally expect a remarkable change in Fermi surface properties. To verify this scenario, we performed specific heat measurements for both Co-doped and Mn-doped samples. The data are presented in Fig. 4c and 4d. All of the data below 10 K can be fitted to $C = \gamma_e T + \beta T^3$ except for the 0.8% Co-doped sample, where $\gamma_e T$ and βT^3 represent electronic and phonon specific heat, respectively. The Sommerfeld coefficient γ_e obtained from these fittings is summarized in Fig. 4b, which shows that γ_e increases strikingly with Co doping, up to ~45 mJ/(mol K^2) for the 1.5% Co-doped sample, but decreases with Mn-doping, down to ~29 mJ/(mol K^2) for 10% Mn-doped sample. The enhancement of γ_e observed in Co-doped Sr_2RuO_4 is likely due to an increase of $N(E_F)$, suggesting that the short-range FM order in Co-doped Sr_2RuO_4 is the result of a Stoner instability induced by electron doping, similar to what happens in the La-doped system[28,29]. That is, electron doping from Co pushes the Fermi level of the Ru $4d_{xy}$ band closer to the vHS.

However, if the mechanism responsible for enhanced FM correlation in both the La-doped system and the Co-doped system is the same, one obvious question remains: why is Co doping of Sr_2RuO_4 so much more effective than La doping at inducing static FM order?

One possibility is that the Co 3*d* orbitals contribute to the Fermi level. Thus Co impurities, whether in the 2+ or 3+ valence state, dope more electrons than La impurities, leading to a faster increase of $N(E_F)$ with Co doping than with La doping. The faster increase of $N(E_F)$ with Co doping can be verified by comparing how γ_e evolves with La doping to how it evolves with Co doping. From data presented in[29], we estimate γ_e of 5% La-doped Sr_2RuO_4 is approximately equal to γ_e of our 1.5% Co-doped sample, indicating that 1.5% Co doping leads to approximately the same increase of $N(E_F)$ as 5% La doping. Noting that the susceptibility of the 1.5% Co-doped sample is ~4–5 times larger than that seen in 5% La-doped Sr_2RuO_4, we find that the Wilson ratio in the Co-doped system is ~4–5 times larger than that in the La-doped system. The stronger FM interactions in Co-doped Sr_2RuO_4, as evidenced by the larger Wilson ratio, could lead to a longer magnetic correlation length in the Co-doped system than in the La-doped system, thus leading to static FM order that is observable by bulk magnetization measurements rather than to enhanced FM fluctuations, which are observed in the La-doped samples.

The observation that Mn doping of Sr_2RuO_4 is more effective than Ti doping at inducing static incommensurate AFM order could help us determine the mechanism responsible for incommensurate AFM order in these two doped systems. If the incommensurate order in Ti-doped samples is the result of an SDW instability as has been suggested[21], then apparently Mn is more effective than Ti at enhancing Fermi surface nesting between the α and β sheets. One possible explanation for this is that Mn increases the size of the α sheet through hole doping, thus improving the nesting between the α and β sheets. Another intriguing possibility is that Ti- and Mn-doped samples involve local moment magnetism. As has been pointed out in Ref. 37, the Curie-Weiss-like behavior of susceptibility and the low-temperature weakly localized state of Ti-doped Sr_2RuO_4 may suggest local moment magnetism in the system. Mn-doped samples also show Curie-Weiss-like behavior above ~200 K and form a low-temperature weakly localized state, the onset of which is coincident with the onset of incommensurate order. Furthermore, the systematic reduction in γ_e with Mn doping (Fig. 4b) suggests that Mn pushes the system towards an insulating ground state. Such a reduction of γ_e has been observed in $Sr_2Ru_{1-x}Ti_xO_4$ above $x = 0.025$[38,39] and in $SrRu_{1-x}Mn_xO_3$ above $x = 0.2$[40]. In both materials, the reduction of γ_e corresponds to a low-temperature weakly localized or insulating state as well as antiferromagnetism. From our results, this is obviously also true for Mn-doped Sr_2RuO_4: the low-temperature weakly localized state and incommensurate AFM order are coupled, which could further suggest local moment magnetism in the system. Further study of this issue is necessary to help us better understand the mechanism responsible for the incommensurate order in Ti- and Mn-doped Sr_2RuO_4.

Finally, let us comment on the unusual behavior observed in the specific heat of 0.8% Co-doped Sr_2RuO_4. As show in Fig. 4d, C/T in this sample exhibits a remarkable upturn at low temperature. This feature was reproduced in two other measured samples with 0.8% Co. Such an upturn is not due to impurities since it disappears for 1.5% doping, but indicative of non-Fermi liquid behavior. This appears to be consistent with the behavior of the low-temperature resistivity of the 0.8% Co-doped sample, as seen from the inset in Fig. 3a. In both the 1.5% Co-doped sample and the undoped sample[41], the T^2 temperature dependence of resistivity associated with Fermi liquid behavior holds for $T < 25$ K. However, the resistivity of the 0.8% Co-doped sample $\propto T^2$ only for $T < 16$ K, indicating that the Fermi liquid temperature in the 0.8% Co-doped sample is lower than that in the 1.5% Co-doped and undoped samples. The lower Fermi liquid temperature in 0.8% Co-doped Sr_2RuO_4 can reasonably be attributed to the combined effects of chemical inhomogeneity and enhanced FM fluctuations from Co doping. Because the doping level is very low, there is undoubtedly inhomogeneity in the distribution of Co in the lattice. Hence, some areas of the crystal will have excess Co, leading to the formation of magnetic droplets with static FM order in these areas. The observation of slight hysteresis in the 0.8% Co-doped isothermal magnetization data shown in Fig. 2d is consistent with the formation of such FM clusters. Other areas of the crystal will have a deficit of Co and will not form these magnetic droplets. Rather, these areas will exhibit enhanced FM fluctuations associated with quantum criticality. The net effect is the observation of a lower Fermi liquid temperature as measured from resistivity and a low-temperature upturn in the specific heat of the 0.8% Co-doped sample. The low-temperature upturn in C/T does not show up in the 1.5% Co-doped sample. This can be attributed to the fact that the 0.8% Co-doped sample is closer to the quantum critical point than the 1.5% Co-doped sample. The higher Fermi liquid temperature observed in 1.5% Co sample is also consistent with this interpretation. We note that a similar behavior is also observed in the La-doped Sr_2RuO_4 system where the non-Fermi liquid behavior in specific heat is observed in the 10% La-doped sample, but not in 13% La-doped sample[29].

In summary, through our studies of Mn- and Co-doped Sr_2RuO_4, we have demonstrated that the superconducting state in Sr_2RuO_4 is much closer than previously believed to static FM order and static incommensurate AFM order. FM cluster glass phase can be triggered in the system with as little as 0.8–1.5% Co doping; this is to be contrasted with the $Ca_{2-x}Sr_xRuO_4$ system, which shows an FM cluster glass phase as x is decreased to 1.5. On the other hand, we find that Mn doping induces short-range, static incommensurate AFM order, similar to the Ti doping effect previously reported. The ordering temperature T_N in Mn-doped samples is much higher than that in Ti-doped samples, indicating that Mn impurities can induce stronger AFM coupling than Ti impurities. Our findings in these two doped systems not only highlight an important role of competing FM and AFM fluctuations in determining superconducting properties of Sr_2RuO_4, but also provide a unique playground for studying the novel physics of orbital-dependent magnetism in strongly correlated materials.

Methods

Single crystal growth and characterization. We have grown single crystals of Mn- and Co-doped Sr_2RuO_4 by the floating-zone method[42]. All single crystals selected for measurement were first screened by x-ray diffraction to ensure phase purity. The successful doping of Mn/Co into the crystals was confirmed by energy-dispersive x-ray spectroscopy (EDXS). For the Mn-doped samples, the nominal concentration of Mn and the measured concentration were comparable, similar to what was found in Ti-doped samples[20]. However, for the Co-doped samples, EDXS analysis showed a significant discrepancy between the nominal Co concentration and the measured Co concentration in the crystals. On average, the nominally 3% Co-doped crystals were found to have a Co concentration of ~1.5% and the nominally 1% Co-doped crystals were found to have a Co concentration of ~0.8%. Although we grew a nominally 10% Co-doped crystal successfully, EDXS analysis showed the Co concentration in the nominally 10% Co-doped samples was comparable to that in the nominally 3% Co-doped samples, indicating Co has a much lower soluble limit than Mn or Ti in Sr_2RuO_4. We used measured doping concentrations in the discussions given above. All magnetization data was collected by a SQUID magnetometer (Quantum Design, model VSM), all resistivity data was taken using the standard four-probe method in a physical property measurement system (PPMS, Quantum Design), and all specific heat data was measured using an adiabatic relaxation method in the PPMS.

Neutron scattering. Neutron diffraction experiments on the 3% Mn doped sample were carried out on HB1 triple-axis spectroscopy stationed in High Flux Isotope Reactor at Oak Ridge National Laboratory.

1. Maeno, Y. *et al.* Superconductivity in a layered perovskite without copper. *Nature* **372**, 532–534 (1994).
2. Ishida, K. *et al.* Anisotropic pairing in superconducting Sr_2RuO_4: Ru NMR and NQR studies. *Phys. Rev. B* **56**, R505–R508 (1997).
3. Nishizaki, S., Maeno, Y., Farner, S., Ikeda, S. & Fujita, T. Evidence for unconventional superconductivity of Sr_2RuO_4 from specific-heat measurements. *J. Phys. Soc. Jpn.* **67**, 560–563 (1998).
4. Mackenzie, A. P. *et al.* Extremely strong dependence of superconductivity on disorder in Sr_2RuO_4. *Phys. Rev. Lett.* **80**, 161–164 (1998).

5. Jin, R. *et al.* Observation of anomalous temperature dependence of the critical current in Pb/Sr_2RuO_4/Pb junctions. *Phys. Rev. B* **59**, 4433–4438 (1999).
6. Rice, T. M. & Sigrist, M. Sr_2RuO_4: an electronic analogue of ^{3}He? *J. Phys.: Condens. Matter* **7**, L643–L648 (1995).
7. Luke, G. M. *et al.* Time-reversal symmetry-breaking superconductivity in Sr_2RuO_4. *Nature* **394**, 558–561 (1998).
8. K. Ishida, K. *et al.* Spin-triplet superconductivity in Sr_2RuO_4 identified by ^{17}O Knight shift. *Nature* **396**, 658–660 (1998).
9. Nelson, K. D., Mao, Z. Q., Maeno, Y. & Liu, Y. Odd-parity superconductivity in Sr_2RuO_4. *Science* **306**, 1151–1154 (2004).
10. Xia, J., Maeno, Y., Beyersdorf, P. T., Fejer, M. M. & Kapitulnik, A. High resolution polar Kerr effect measurements of Sr_2RuO_4: evidence for broken time-reversal symmetry in the superconducting state. *Phys. Rev. Lett.* **97**, 167002 (2006).
11. Kidwingira, F., Strand, J. D., Van Harlingen, D. J. & Maeno, Y. Dynamical superconducting order parameter domains in Sr_2RuO_4. *Science* **314**, 1267–1271 (2006).
12. Jang, J. *et al.* Observation of half-height magnetization steps in Sr_2RuO_4. *Science* **331**, 186–188 (2011).
13. Mackenzie, A. P. & Maeno, Y. The superconductivity of Sr_2RuO_4 and the physics of spin-triplet pairing. *Rev. Mod. Phys.* **75**, 657–712 (2003).
14. Maeno, Y., Kittaka, S., Nomura, T., Yonezawa, S. & Ishida, K. Evaluation of spin-triplet superconductivity in Sr_2RuO_4. *J. Phys. Soc. Jpn.* **81**, 011009 (2012).
15. Vaknin, D. *et al.* Antiferromagnetism in La_2CuO_{4-y}. *Phys. Rev. Lett.* **58**, 2802–2805 (1987).
16. de la Cruz, C. *et al.* Magnetic order close to superconductivity in the iron-based layered $LaO_{1-x}F_xFeAs$ systems. *Nature* **453**, 899–902 (2008).
17. Bauer, E. *et al.* Heavy fermion superconductivity and magnetic order in noncentrosymmetric $CePt_3Si$. *Phys. Rev. Lett.* **92**, 027003 (2004).
18. Sidis, Y. *et al.* Evidence for incommensurate spin fluctuations in Sr_2RuO_4. *Phys. Rev. Lett.* **83**, 3320–3323 (1999).
19. Mazin, I. I. & Singh, D. J. Competition in layered ruthenates: ferromagnetism versus antiferromagnetism and triplet versus singlet pairing. *Phys. Rev. Lett.* **82**, 4324–4327 (1999).
20. Minakata, M. & Maeno, Y. Magnetic ordering in Sr_2RuO_4 induced by nonmagnetic impurities. *Phys. Rev. B* **63**, 180504(R) (2001).
21. Braden, M. *et al.* Incommensurate magnetic ordering in $Sr_2Ru_{1-x}Ti_xO_4$. *Phys. Rev. Lett.* **88**, 197002 (2002).
22. Mazin, I. I. & Singh, D. J. Ferromagnetic spin fluctuation induced superconductivity in Sr_2RuO_4. *Phys. Rev. Lett.* **79**, 733–736 (1997).
23. Miyake, K. & Narikiyo, O. Model for unconventional superconductivity of Sr_2RuO_4: effect of impurity scattering on time-reversal breaking triplet pairing with a tiny gap. *Phys. Rev. Lett.* **83**, 1423–1426 (1999).
24. Fang, Z. & Terakura, K. Magnetic phase diagram of $Ca_{2-x}Sr_xRuO_4$ governed by structural distortions. *Phys. Rev. B* **64**, 020509(R) (2001).
25. Nomura, T. & Yamada, K. Roles of electron correlations in the spin-triplet superconductivity of Sr_2RuO_4. *J. Phys. Soc. Jpn.* **71**, 1993–2004 (2002).
26. Imai, T., Hunt, A. W., Turber, K. R. & Chou, F. C. ^{17}O NMR evidence for orbital dependent ferromagnetic correlations in Sr_2RuO_4. *Phys. Rev. Lett.* **81**, 3006–3009 (1998).
27. Braden, M. *et al.* Inelastic neutron scattering study of magnetic excitations in Sr_2RuO_4. *Phys. Rev. B* **66**, 064522 (2002).
28. Kikugawa, N. *et al.* Rigid-band shift of the Fermi level in the strongly correlated metal: $Sr_{2-y}La_yRuO_4$. *Phys. Rev. B* **70**, 060508(R) (2004).
29. Kikugawa, N., Bergemann, C., Mackenzie, A. P. & Maeno, Y. Band-selective modification of the magnetic fluctuations in Sr_2RuO_4: a study of substitution effects. *Phys. Rev. B* **70**, 134520 (2004).
30. Carlo, J. P. *et al.* New magnetic phase diagram of $(Sr,Ca)_2RuO_4$. *Nature Mater.* **11**, 323–328 (2012).
31. Nakatsuji, S. *et al.* Heavy-mass fermi liquid near a ferromagnetic instability in layered ruthenates. *Phys. Rev. Lett.* **90**, 137202 (2003).
32. Kanbayasi, A. Magnetic properties of $SrRuO_3$ single crystal. *J. Phys. Soc. Jpn.* **41**, 1876–1878 (1976).
33. Xia, J., Siemons, W., Koster, G., Beasley, M. R. & Kapitulnik, A. Critical thickness for itinerant ferromagnetism in ultrathin films of $SrRuO_3$. *Phys. Rev. B* **79**, 140407(R) (2009).
34. Agterberg, D. F., Rice, T. M. & Sigrist, M. Orbital dependent superconductivity in Sr_2RuO_4. *Phys. Rev. Lett.* **78**, 3374–3377 (1997).
35. Deguchi, K., Mao, Z. Q., Yaguchi, H. & Maeno, Y. Gap structure of the spin-triplet superconductor Sr_2RuO_4 determined from the field-orientation dependence of the specific heat. *Phys. Rev. Lett.* **92**, 047002 (2004).
36. Friedt, O. *et al.* Structural and magnetic aspects of the metal-insulator transition in $Ca_{2-x}Sr_xRuO_4$. *Phys. Rev. B* **63**, 174432 (2001).
37. Bergemann, C., Mackenzie, A. P., Julian, S. R., Forsythe, D. & Ohmichi, E. Quasi-two-dimensional Fermi liquid properties of the unconventional superconductor Sr_2RuO_4. *Adv. Phys.* **52**, 639–725 (2003).
38. Pucher, K. *et al.* Transport, magnetic, thermodynamic, and optical properties in Ti-doped Sr_2RuO_4. *Phys. Rev. B* **65**, 104523 (2002).
39. Kikugawa, N. & Maeno, Y. Non-Fermi-liquid behavior in Sr_2RuO_4 with nonmagnetic impurities. *Phys. Rev. Lett.* **89**, 117001 (2002).
40. Yamaji, A., Yokoyama, M., Nishihara, Y., Narumi, Y. & Kindo, K. Specific-heat study for ferromagnetic and antiferromagnetic phases in $SrRu_{1-x}Mn_xO_3$. *J. Phys.: Conf. Ser.* **200**, 012232 (2010).
41. Maeno, Y. *et al.* Two-dimensional Fermi liquid behavior of the superconductor Sr_2RuO_4. *J. Phys. Soc. Jpn.* **66**, 1405–1408 (1997).
42. Mao, Z. Q., Maeno, Y. & Fukazawa, H. Crystal growth of Sr_2RuO_4. *Mater. Res. Bull.* **35**, 1813–1824 (2000).

Acknowledgements

The work is supported by the NSF under grant DMR-1205469 and the LA-SiGMA program under award #EPS-1003897. X. K. acknowledges the financial support from the start-up funds at Michigan State University. Research at ORNL's High Flux Isotope Reactor was sponsored by DOE basic Energy Sciences, Scientific User Facilities Division. The authors are grateful to L. Zheng and X.S. Wu for informative discussions.

Author contributions

J.E.O. conducted single crystal growth, structural characterization and magnetization and specific heat measurements. J.L. and J.H. contributed to resistivity and specific heat measurements. J.P. contributed to crystal growth in part. Neutron scattering measurements were carried out by M.Z., M.M. and X.K. Z.Q.M. supervised the project and co-wrote the manuscript with J.E.O. All authors reviewed and commented on the manuscript.

Additional information

Supplementary information accompanies this paper at http://www.nature.com/scientificreports

Competing financial interests: The authors declare no competing financial interests.

How to cite this article: Ortmann, J.E. *et al.* Competition Between Antiferromagnetism and Ferromagnetism in Sr_2RuO_4 Probed by Mn and Co Doping. *Sci. Rep.* **3**, 2950; DOI:10.1038/srep02950 (2013).